Neuron
Article

Inactivation of the Parietal Reach Region Causes Optic Ataxia, Impairing Reaches but Not Saccades

Eun Jung Hwang,[1,*] Markus Hauschild,[1] Melanie Wilke,[1,2,3] and Richard A. Andersen[1]
[1]Division of Biology, California Institute of Technology, Pasadena, CA 91125, USA
[2]Department of Cognitive Neurology, University of Goettingen, Goettingen 37075, Germany
[3]German Primate Center, Leibniz Institute for Primate Research, Goettingen 37077, Germany
*Correspondence: eunjung@caltech.edu
http://dx.doi.org/10.1016/j.neuron.2012.10.030

SUMMARY

Lesions in human posterior parietal cortex can cause optic ataxia (OA), in which reaches but not saccades to visual objects are impaired, suggesting separate visuomotor pathways for the two effectors. In monkeys, one potentially crucial area for reach control is the parietal reach region (PRR), in which neurons respond preferentially during reach planning as compared to saccade planning. However, direct causal evidence linking the monkey PRR to the deficits observed in OA is missing. We thus inactivated part of the macaque PRR, in the medial wall of the intraparietal sulcus, and produced the hallmarks of OA, misreaching for peripheral targets but unimpaired saccades. Furthermore, reach errors were larger for the targets preferred by the neural population local to the injection site. These results demonstrate that PRR is causally involved in reach-specific visuomotor pathways, and reach goal disruption in PRR can be a neural basis of OA.

INTRODUCTION

The posterior parietal cortex (PPC) is an important interface between sensory and motor cortices, integrating multimodal sensory and motor signals to process spatial information for a variety of functions including guiding attention, making decisions, understanding actions, and planning movements (Andersen et al., 1997; Bisley and Goldberg, 2010; Caminiti et al., 2010; Corbetta et al., 2000; Gold and Shadlen, 2007; Green and Angelaki, 2010; Rizzolatti and Sinigaglia, 2010). Correspondingly, lesions in human PPC can lead to complex syndromes consisting of an inability to attend, perceive, and react to stimuli in the visual field contralateral to the lesion, an inability to voluntarily control eye gaze, and an inability to coordinate visually elicited hand movements (Caminiti et al., 2010; D'Esposito, 2003; Hyvärinen, 1982; Mesulam, 2000). The impaired coordination of visually elicited hand movements is known as optic ataxia (OA) (Garcin et al., 1967; Perenin and Vighetto, 1988; Rossetti et al., 2003).

OA can occur in isolation from the other parietal symptoms and can be dissociated from motor, somatosensory, visual acuity, or visual field deficits (Garcin et al., 1967; Perenin and Vighetto, 1988; Rossetti et al., 2003). For example, when OA patients are asked to reach to visual objects presented in the ataxic field, i.e., in the periphery of the contralesional visual field, the reaches are often deflected from the target objects and pulled toward the gaze location (Blangero et al., 2010; Jackson et al., 2005; Milner et al., 1999). Yet, OA patients may show no significant perceptual impairment in judging visual stimulus position in the ataxic field (Buxbaum and Coslett, 1997, 1998; Perenin and Vighetto, 1988; Schindler et al., 2004). Moreover, OA patients can make saccade movements to visual objects in the ataxic field with normal accuracy (Khan et al., 2009; Trillenberg et al., 2007). Although the reach-specific deficits associated with OA suggest that PPC may include distinct areas dedicated to the control of reaching movements, the typical extent and variability of the lesions in human patients hinder pinpointing the underlying neural substrates (Goodale and Milner, 1992; Karnath and Perenin, 2005; Perenin and Vighetto, 1988; Rossetti et al., 2003). A more precise way to identify the neural substrate responsible for OA would be to cause controlled lesions in a circumscribed area in nonhuman primates and compare its behavioral effects with the known OA symptoms. If the functional properties of that circumscribed area (e.g., behavioral parameters encoded by neurons in that area) are characterized, the computational mechanisms underlying the OA symptoms could also be elucidated.

Several areas in human and nonhuman primate PPC have been implicated in visuomotor control for distinct effectors based on their neural activity patterns elicited by specific types of movements that the subject plans to make (Andersen and Buneo, 2002; Caminiti et al., 2010; Culham et al., 2006; Grefkes and Fink, 2005). For example, in monkeys, the anterior intraparietal area (AIP), the lateral intraparietal area (LIP), and the parietal reach region (PRR) contain neurons that are specifically sensitive to grasp, saccade, and reach movements, respectively. The monkey PRR is a functionally defined region in which the majority of neurons are spatially tuned to the reach goal direction and the activity is stronger during reach than saccade planning (Snyder et al., 1997). Anatomically, this region includes the anterior wall of the parieto-occipital sulcus (POS) and the medial wall of the intraparietal sulcus (IPS) (Battaglia-Mayer et al., 2000; Galletti et al., 1997; Kalaska et al., 1983; Snyder et al., 1997). The reach-specific activity in PRR suggests that it encodes the subject's intended reach goal, an essential parameter for goal-directed reaching, and thus lesion to this region might affect

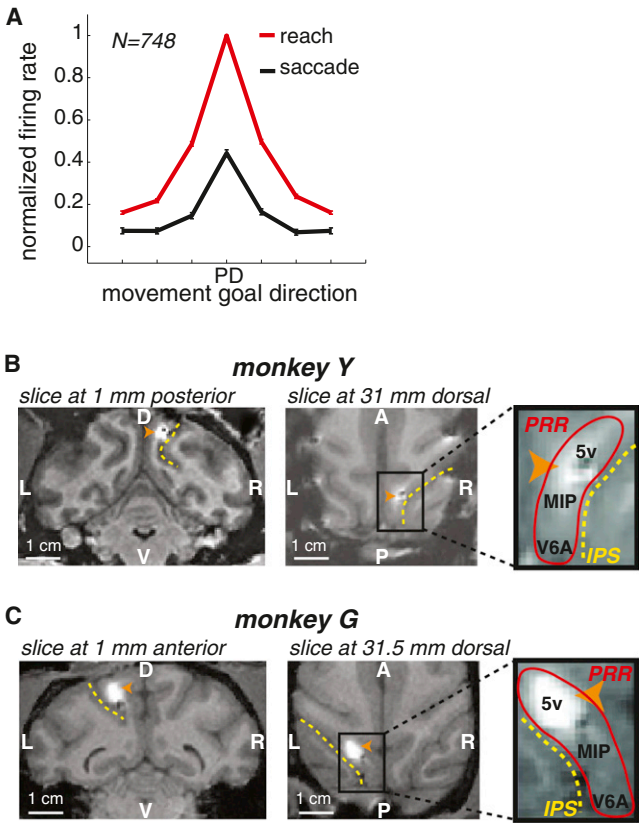

Figure 1. The Functional Property and the Anatomical Location of the Parietal Reach Region

(A) The average firing rate (mean ± SEM) of 748 PRR neurons as a function of the planned reach versus saccade goal direction. PD stands for the preferred direction.

(B) Left: the coronal view of the inactivation area (center: 1 mm posterior, 5 mm lateral, and 31 mm dorsal to the stereotaxic zero point) in monkey Y. The left, right, dorsal, and ventral directions are labeled as L, R, D, and V, respectively. The arrow points to the inactivated area that appears brighter due to the injection of the MRI contrast agent gadolinium. The yellow dotted line indicates the intraparietal sulcus (IPS). Middle: the horizontal view. The anterior and posterior directions are labeled as A and P, respectively. Right: the enlarged horizontal view. The red contour indicates the estimated boundary of PRR, which includes areas V6A, MIP, and 5v.

(C) The same as (B) but for monkey G. The inactivation center was 1 mm anterior, 7 mm lateral, and 31.5 mm dorsal to the stereotaxic zero point. The spread of gadolinium was larger in monkey G than Y because monkey G was injected with double the amount of gadolinium.

reaches but not saccades, similar to OA. Moreover, the goal representation in the monkey PRR is in gaze-centered coordinates, which can account for the observation that reach errors in OA depend on the target location in relation to gaze (Batista et al., 1999; Khan et al., 2005; Pesaran et al., 2006). However, direct causal evidence linking the monkey PRR to the deficits observed in OA has not been demonstrated. Thus, this study aimed to test the hypothesis that controlled lesions of the monkey PRR would produce OA-like symptoms, deficits specifically in reaching to peripheral targets but not reaching to central targets or saccades.

RESULTS

To test this hypothesis, we investigated how PRR inactivation affects goal-directed movements in two macaque monkeys (Y and G). We alternated between inactivation and control sessions spaced at least 24 hr apart (15 inactivation sessions in total for monkey Y and 19 for monkey G) (Experimental Procedures and see Table S1 available online). Because unilateral lesions are sufficient to cause OA in human patients, we inactivated only the right hemisphere in monkey Y and the left hemisphere in monkey G (Perenin and Vighetto, 1988). Both monkeys used the arm opposite to the inactivated hemisphere for reaching. In the beginning of each inactivation session, we injected typically 5 μl of muscimol, a $GABA_A$ agonist that suppresses local neuronal activity, through an acutely inserted cannula (Martin and Ghez, 1999). The inactivation cannula was inserted at an almost constant location where we previously recorded a large number of neurons satisfying the functional criteria of PRR that firing rate is more strongly tuned to reach goal direction than to saccade direction (Figure 1A) (Snyder et al., 1997). We visualized the inactivated area through MRI after injecting the MRI-visible contrast agent gadolinium, known to faithfully reflect the spread of muscimol (Heiss et al., 2010). As indicated by the gadolinium spread, our inactivation was contained within a small volume in the medial wall of IPS, a part of PRR (Figures 1B and 1C). Anatomically, the inactivated area may overlap with the medial intraparietal area (MIP) and/or the ventral part of area 5 (5v). Because of this ambiguity, we hereafter refer to the inactivated area simply as "PRR."

The functional properties of PRR neurons, if causal, predict that PRR inactivation would distort the intended reach goals, which in turn would affect reach endpoint locations. Moreover, the effect would be selective for reaching movements. To test these predictions, we first compared the effects of PRR inactivation on reach and saccade endpoints in memory-guided reach and saccade tasks (seven controls and six inactivations for monkey Y, six and six for monkey G; Figure 2A). Figure 2B displays the reach and saccade endpoints from representative inactivation and control sessions. In comparison to the control session, reaches in the inactivation session ended short of the targets, i.e., reaches were hypometric for several target locations (see Figure S1A for trajectory information). In contrast, the inactivation saccade endpoints were not noticeably different from the control saccade endpoints. Note that the upward shift of the memory-guided saccade endpoints, a phenomenon that has been well documented in previous work (Gnadt et al., 1991), occurred irrespective of inactivation.

Accordingly, in both monkeys, the average reach amplitude but not saccade amplitude differed significantly between the inactivation and control sessions (t test, $p < 0.01$; Experimental Procedures). Figures 2C and 2D show the average reach and saccade amplitudes across all control versus inactivation trials pooled across all sessions for each target location and each monkey, respectively. For all target locations, the inactivation reach amplitude was significantly shorter than the control reach amplitude in both monkeys (t test, $p < 0.01$, multiple comparison corrected; Experimental Procedures). Besides pooling trials across all sessions, we also examined the inactivation effects

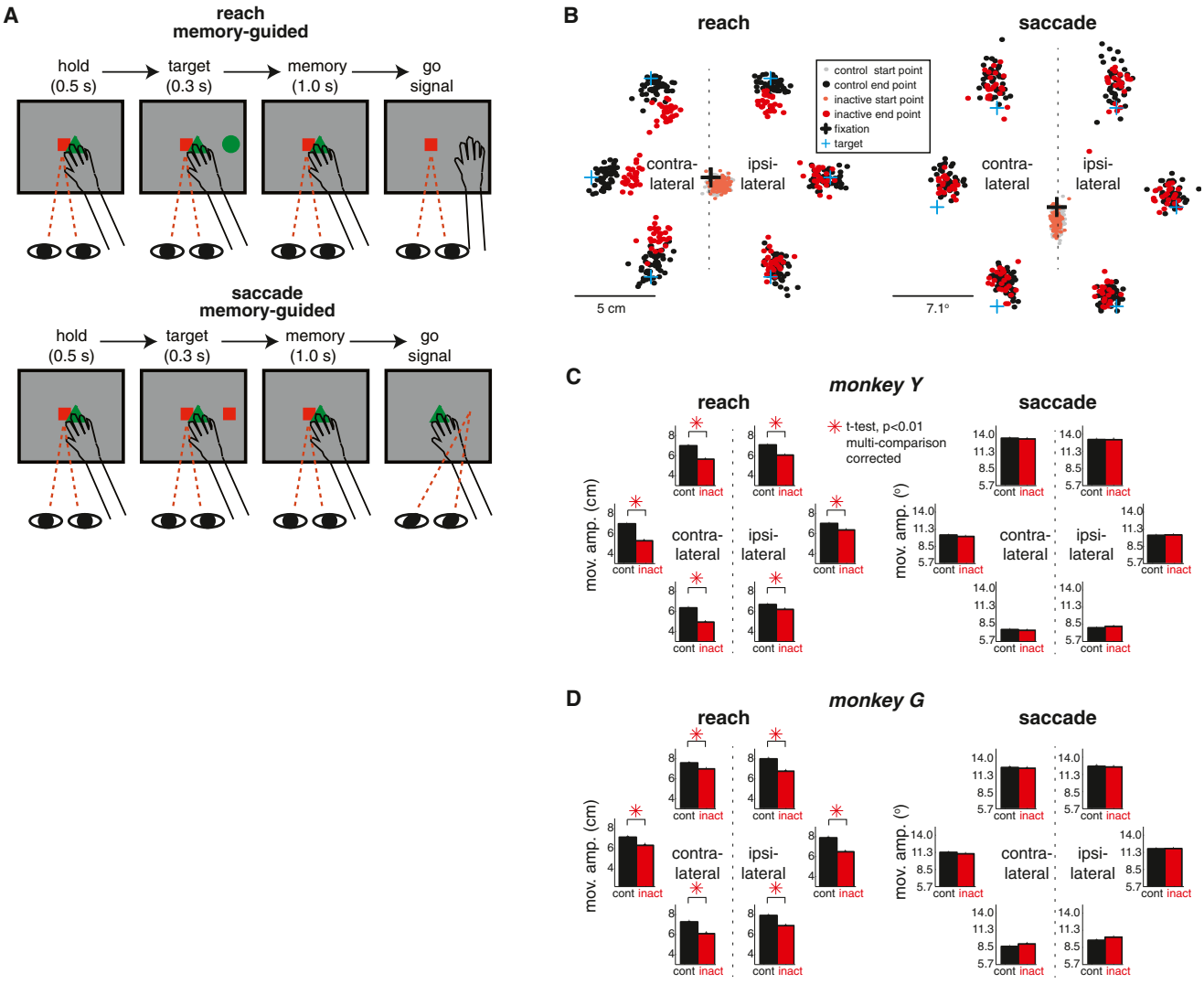

Figure 2. The Inactivation of PRR Causes Reach but Not Saccade Deficits

(A) Temporal sequence of the memory-guided reach and saccade tasks. The monkey reaches or saccades to the remembered location of a target. The red square and green triangle in the center are eye and hand fixation targets, respectively. The green circle in the periphery is the reach target and the red square in the periphery is the saccade target.

(B) Left: the reach endpoints for six targets in a typical inactivation (red) versus control (black) session (1 day before and after the inactivation session). Right: the saccade endpoints from the same sessions. The dots in lighter colors in the center indicate the starting points.

(C) Left: the average reach amplitude (mean ± SEM) across all inactivation (red) versus control (black) sessions for each of the six targets in monkey Y. Right: the average saccade amplitude (mean ± SEM). Note that SEMs are too small to be noticeable. The direction is normalized relative to side of injection.

(D) The same as (C) but for monkey G. See also Figure S1.

on a per session basis (Figures S1B and S1C). The analysis clearly showed that the reach deficits caused by inactivation were reliable and robust across all sessions. In contrast, the saccade amplitude was not significantly affected by the inactivation for any target location (t test, $p > 0.01$; all targets in both monkeys). The reach-specific effect rules out the possibility that PRR inactivation impaired the spatial perception of stimuli in the periphery. Rather, the result corroborates our prediction that PRR inactivation disrupts the reach goal information and affects visuomotor spatial control selectively for reaches.

The hypometric reaches show striking resemblance to the misreaching pattern found in human OA patients suffering from major parietal lobe damage in a similar experimental setup (Blangero et al., 2010; Milner et al., 1999; Ratcliff and Davies-Jones, 1972). Intriguingly, the human OA misreaching is negligible when targets are in the central visual field (Jackson et al., 2005; Perenin and Vighetto, 1988). Thus, when the patients are allowed to foveate the reach target before reaching, the misreaching is significantly reduced (Blangero et al., 2010; Caminiti et al., 2010; Karnath and Perenin, 2005; Perenin and Vighetto,

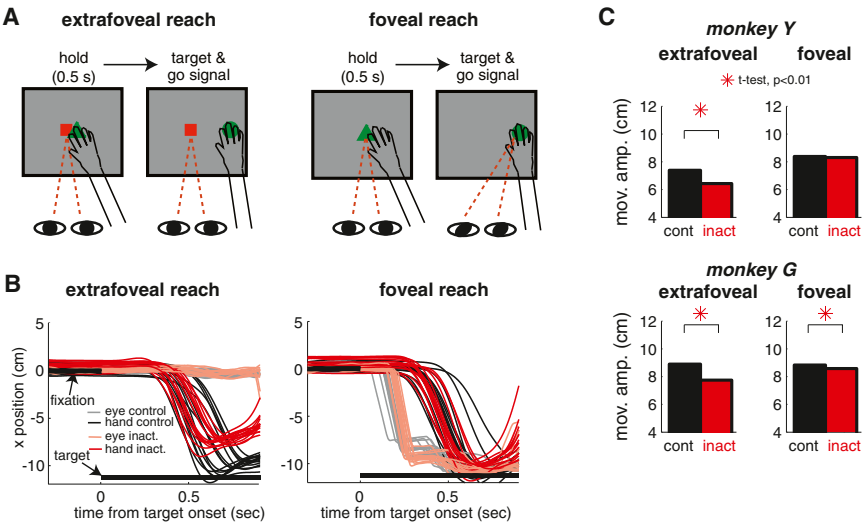

Figure 3. The Inactivation of PRR Causes Misreaching to Peripheral but Not Central Targets Similar to Optic Ataxia

(A) Extrafoveal versus foveal reaches. The monkey reaches to the green circle. Under the extrafoveal condition, eyes are fixated on the red square while reaching. Under the foveal condition, eyes are not constrained.

(B) Sample hand and eye traces of 15 trials for a single target location in a typical inactivation (dark red/reach and light red/saccade) versus control session (dark black/reach and light black/saccade). Under the extrafoveal condition, the eyes are fixated on the center fixation target. Under the foveal condition, the eyes initially fixate at the center hand position, jump to the target location as soon as the target is presented, and stay until the hand reaches the target.

(C) The average reach amplitude (mean ± SEM) across all inactivation (red) versus control (black) trials. Trials for all six target locations were combined.

1988; Rossetti et al., 2003). To test whether PRR inactivation produces such selective deficits similar to human OA, we compared deficits in reaching to visible targets between two different gaze conditions (seven controls and six inactivations for monkey Y, 13 and 12 for monkey G; Figure 3A; Experimental Procedures). Here, differently from the memory-guided reaches tested in the above section, the monkeys were allowed to reach any time after the target onset and the target remained visible during reaching. Under the extrafoveal condition, reach targets were in the peripheral visual field by requiring the monkeys to fixate their eyes on the central eye fixation target throughout the trial. Under the foveal condition, the eyes were not constrained in any way so that the monkeys would foveate reach targets through stereotypical eye-hand coordination (Cisek and Kalaska, 2004; Prablanc et al., 1986). Indeed, under the foveal condition, the monkeys first looked at the central hand start position, made a saccade to the target when the target was presented, and maintained the target foveation until the end of a reach (Figure 3B). Similar to human OA, we found that the reach amplitude reduction by PRR inactivation was significantly smaller in the foveal than extrafoveal condition for both monkeys (Figure 3C; t test, $p < 0.01$, Experimental Procedures). Thus, so far, we reproduced three major OA symptoms: (1) misreaching for visual targets in the peripheral visual field, (2) no deficits in saccades, and (3) reduced reaching errors in the central visual field. These results support our prediction that PRR can be a neural substrate responsible for the OA misreaching.

The reaching impairment by PRR inactivation was not limited to memory-guided reaches; in the task under the extrafoveal condition in the above section, the monkeys immediately reached to the visible target without a memory period, yet significant hypometria was caused by PRR inactivation (t test, $p < 0.01$ for both monkeys). This result shows that misreaching is not due to spatial memory being impaired. It is also notable that the reaching impairment was not limited to reaches whose goals are directly cued by illuminating the target location; instead, misreaching manifested even when the goal was indirectly inferred from a symbol after a learned association rule between the symbols and target locations (Figure S2). This result is consistent with the finding that PRR neurons encode symbolically cued reach goals similarly to directly cued reach goals (Hwang and Andersen, 2012). Therefore, the hypometria reflects a general deficit of reach goal representation as opposed to a selective impairment of direct visuomotor transformation.

Human OA patients with unilateral lesions typically show stronger impairment for reaches to targets in the contralesional field, consistent with the lateralized spatial representation in human PPC (Blangero et al., 2010; Perenin and Vighetto, 1988). To compare, we computed the average inactivation effect for the contralesional versus ipsilesional targets, respectively. The inactivation effect was computed as the percentage reduction of the reach amplitude from the control baseline amplitude (Experimental Procedures). Although reach amplitudes in both monkeys were significantly affected in both hemifields (t test, $p < 0.01$), the effect was stronger for the contralesional field for monkey Y, but it was stronger for the ipsilesional field for monkey G (Figures 2C, 2D, and 4A). This puzzling difference between the two monkeys was resolved when we examined the reach direction represented by the neurons in the local area that we inactivated in each monkey separately. Figure 4B displays the histogram of the preferred direction of the spiking units recorded in a proximal area (within ~1 mm) from the inactivation cannula prior to the inactivation experiment during the memory-guided reach task. This analysis revealed that the inactivated PRR area contained more neurons with their preferred direction in the contralesional field in monkey Y and more in the ipsilateral field in monkey G. These biases of the reach direction representation were consistent with the biases of the inactivation effects between the two hemifields. That is, in both monkeys, a stronger inactivation effect was found in the more strongly represented hemifield. To further elucidate the link between neural representation and behavior, we examined the relation between the population activity strength and the reach amplitude reduction

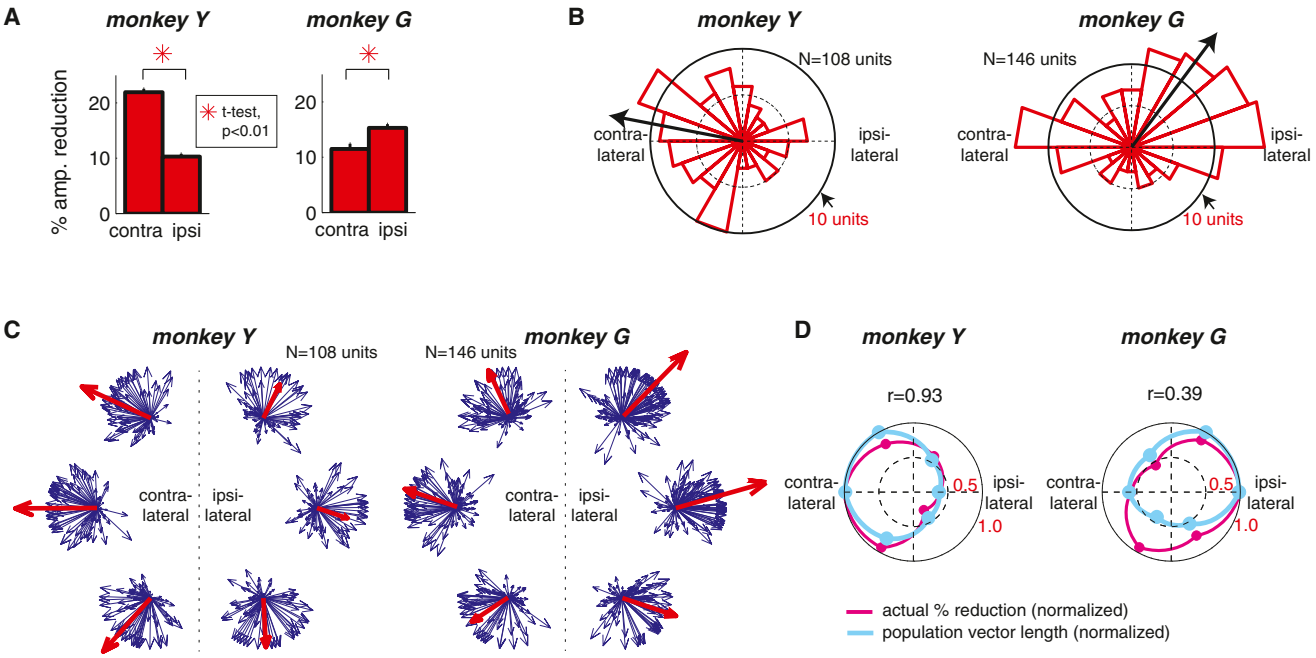

Figure 4. The Directional Bias of Local PRR Neurons Explains the Bias of the Inactivation Deficit

(A) Average reach amplitude reduction after inactivation (mean ± SEM) for the contralesional versus ipsilesional targets in the memory-guided reach task.

(B) Histogram of the preferred reach directions of spiking units within 1 mm from the inactivation cannula. Arrows indicate the population mean.

(C) Population vector (red arrow), i.e., the sum of all blue arrows, each scaled down by a factor of 20, for each of the six targets. Each blue arrow represents the activity of an individual spiking unit in its preferred direction with the amplitude of the mean activity for a given target.

(D) Average reach amplitude reduction (magenta) and population vector amplitude (cyan) for each of the six targets. Both lines are normalized respectively so that their maximum is 1. See also Figure S3.

across the six target locations (Experimental Procedures). The strength of the population activity was estimated from the population vector, the sum of the preferred directions of the neuronal ensemble, weighted by their respective firing rates for a given target location (Figure 4C) (Georgopoulos et al., 1986). We found that the length of the population vector closely matched the relative inactivation effect on the reach amplitude. The Pearson's correlation coefficient between the reach amplitude reduction and population vector amplitude was 0.93 and 0.39 for monkey Y and G, respectively (Pearson's correlation coefficient test, $p < 0.01$; Figure 4D).

When constructing the population vector from a larger volume of PRR, the bias of the reach direction representation in PRR became weaker (Figure S3A). The muscimol concentration in the brain and thus its effect decreases with the distance from the injection center. Given the muscimol volume (5 μl) and post-injection time (35–169 min), we estimate the muscimol spread to reach up to ~2.1 mm from the injection center (Heiss et al., 2010; Martin and Ghez, 1999). As expected from the limited spatial spread of muscimol, the correlation between the population activity strength and the inactivation effect decreased as the area over which we included spiking units expanded farther from the inactivation cannula (Figures S3B–S3D). The tight spatial correlation between the inactivation effect and the local neural activity provides further evidence for the causal involvement of PRR in goal-directed reaching movements.

DISCUSSION

In the current study, using targeted reversible inactivation and electrophysiological recording of a circumscribed and functionally well-defined area in the monkey PRR, we elucidated a neural basis of OA. PRR inactivation produced a very robust deficit in the accuracy of reaches but not saccades, providing direct causal evidence linking monkey PRR to deficits seen in OA. Further strengthening the causal link, the spatial modulations of the inactivation effect and the local population activity were tightly correlated. These results demonstrate that disrupted reach goal representation in the human homolog of PRR might be a cause for OA (Caminiti et al., 2010).

Relation to Human Studies

The issue of which area(s) in the human brain is homologous to the monkey PRR is an ongoing research topic. Connolly et al. (2003) reported that the precuneus region responded preferentially when human subjects made pointing movements as compared to saccades to the same spatial location, raising the possibility of the precuneus region being homologous to monkey PRR. Other fMRI studies confirmed the pointing/reach-selective activity in the precuneus region but reported additional brain areas with selective activity for reaching such as the inferior parietal lobule (IPL), the superior parietal lobule (SPL), the medial intraparietal sulcus (mIPS), and a region lateral to the precuneus

called the parieto-occipital junction (POJ) (Astafiev et al., 2003; Cavina-Pratesi et al., 2010; Filimon et al., 2009; Prado et al., 2005). Therefore, multiple areas in the human PPC appear to be a putative homolog of the monkey PRR.

These putative homologs of the monkey PRR coincide with, or are in the vicinity of, common lesion sites observed in OA patients (Culham et al., 2006). Perenin and Vighetto (1988) originally suggested that the common lesion sites in OA patients were the IPS, the SPL, and the IPL. A more recent lesion overlap analysis with a large number of unilateral OA patients revealed three somewhat different foci, one in the precuneus, one in the superior occipital gyrus near the POJ, and one in the SPL (Culham et al., 2006; Karnath and Perenin, 2005). As such, multiple areas implicated for OA overlap with the putative human PRR.

Prado et al. (2005) proposed that OA patients who have deficits when reaching to peripheral targets but not to central targets have lesions specifically in the POJ. This proposal was based on their observation that the POJ was activated only when the reach was made to a peripheral target, while the mIPS was activated during a reaching task regardless of whether the reach target appeared in central or peripheral vision. In line with this proposal, repetitive TMS in humans over a region near the POJ/precuneus (named ''superior parietal occipital cortex'') impaired reaches to peripheral targets, with reaches ending short of the targets (Vesia et al., 2010). This deficit is very similar to the effect of our monkey PRR inactivation, providing further evidence for the functional similarity between the human precuneus/POJ and the monkey PRR. However, our inactivation site is more anterior and lateral to the precuneus/POJ region. Although homologous areas in the human and monkey brains may not always topographically correspond to each other, the topological discrepancy calls for further functional, anatomical, and cytoarchitectural comparisons between the two areas (Mantini et al., 2012).

Foveal versus Extrafoveal Reaches

Foveal reaches differ from extrafoveal reaches in at least two main aspects: the foveal capture of the target and an accompanying saccade to the target. At present, it is unknown if only one of the two or both contribute to the lack of PRR inactivation effect on foveal reaches. However, if the monkey PRR is functionally similar to the human POJ, the foveal capture of the target is probably the determinant (Prado et al., 2005). Nevertheless, the exact mechanism remains to be demonstrated.

Effector-Specific Spatial Representations in PPC

Several areas in human and nonhuman primate PPC have been implicated in the visuomotor control of distinct effectors based on their effector-specific neural activity (Levy et al., 2007; Murata et al., 1996; Snyder et al., 1997). In monkeys, PRR has been implicated in the control of arm reaching, LIP for saccades, and AIP for grasping. Consistent with the neural activity, it has been shown that LIP inactivation produces oculomotor and/or attention impairments (Li et al., 1999; Liu et al., 2010), and AIP inactivation produces abnormal grasps (Gallese et al., 1994). However, until now there has not been any direct causal evidence for PRR's selective involvement in reaching. The current study shows that PRR inactivation produces impairments in arm reaching but not saccades. The reach-specific effects convincingly support the view that PPC includes separate visuomotor pathways for different motor functions and that the spatial representation in PRR genuinely reflects the reach intention, driving goal-directed reaches.

Limitations of the Current Study

Given various experimental constraints, we could not test the full range of deficits found in human OA such as the stronger or exclusive deficits on the contralesional arm, the exacerbated deficits by removing the visual feedback of the hand, or the impaired online corrections of reaching movements (Perenin and Vighetto, 1988; Rossetti et al., 2003). Nor do we expect that the inactivated area in our study would account for all known deficits. For instance, in contrast to reports of OA in humans, our inactivation induced no increase in reaction times or movement times (Figures S4A and S4B) (Perenin and Vighetto, 1988; Pisella et al., 2000; Rossetti et al., 2003). Accordingly, we do not claim that our inactivated area is the sole area responsible for OA. Instead, other deficits in human OA may result from a variety of lesions in PPC. Especially given that successful control of goal-directed reaches requires not only accurate goal information but also accurate hand position information to compute the reach vector before and during reaches, misreaching could theoretically also occur with lesions in areas that compute the hand position or the reach vector. Converging evidence in monkeys indicates that the dorsal area 5 (5d) in PPC encodes the current hand position estimate (Mulliken et al., 2008). Thus, lesions in 5d may also produce misreaching behavior, albeit with a different deficit pattern. This remains to be shown.

EXPERIMENTAL PROCEDURES

Two male adult monkeys (Macaca Mulatta), weighing between 9 and 10 kg, were tested. All surgical and animal care procedures were performed in accordance with NIH guidelines and were approved by the California Institute of Technology Animal Care and Use Committee.

Reversible Inactivation

To perform a reliable correlation analysis between the behavioral effects of inactivation and the underlying neural response properties, we inactivated a relatively constant region across sessions. We previously recorded a large number of PRR neurons in this area that satisfied the functional criteria that the reach direction tuning was stronger than the saccade direction tuning (Figure 1A). The point where the cannulae penetrated the tissue above the brain was constant, (7.5L, 5P mm) and (12.5L, 5P mm) in stereotaxic coordinates for monkey Y and G, respectively. We lowered the cannulae 9 mm and 10.5 mm on average for monkey Y and G. The depth varied only within ±0.5 mm across sessions. The resulting final position of the cannulae was at approximately 4 ± 0.5 mm from the cortical surface estimated as the depth at which we encountered the first neuronal activity. From the MR imaging of the gadolinium spread, we estimated that the center of inactivation area was at (5L, 1P mm) and (7L, 1A mm) in stereotaxic coordinates for monkey Y and G, respectively. These values differ from the initial penetration points because the cannulae were not normal but slightly tilted with respect to the horizontal stereotaxic plane for monkey Y and G. The inactivation was contained within the medial wall of the midposterior portion of the IPS. The medial wall of the IPS includes two anatomically distinct areas, the medial intraparietal area (MIP) and the ventral part of area 5 (5v) (Colby et al., 1988; Lewis and Van Essen, 2000; Saleem and Logothetis, 2012). The distinction between MIP and 5v is based on their myeloarchitecture, and the boundary between the two areas reported in the literature ranges from approximately a quarter to half

way along the IPS from the posterior end. In the absence of histology, we cannot determine the precise boundary of these two areas and, thus, do not know whether the inactivated area was MIP, 5v, or both.

Injection Details

In each inactivation session, a stainless steel beveled-tip cannula (28–30 GA, Plastic One) affixed to a microdrive (NLX18, Neuralynx) was acutely lowered to the aforementioned constant location. Then, typically 5 μl (range: 3.5–10) of muscimol solution (5 mg/ml, pH ~7.4) was injected at 1 μl/min using a 100 μl gas-tight Hamilton syringe and a micropump system (Harvard Apparatus). The behavioral experiment began 35–60 min after the injection started and lasted up to 3 hr, well within the accepted time for muscimol action (Arikan et al., 2002). These experimental parameters for individual sessions are listed in Table S1.

We alternated between inactivation and control sessions. They were typically spaced 24 hr apart. Exceptions were two inactivation sessions with a 2 day separation from the previous control session, and four control sessions with a 3–9 day separation from the previous inactivation sessions. The recovery of function in control sessions was visually noticeable in terms of the reach endpoint accuracy in the interleaved control sessions (Figures S1B, S1C, and S4D). In a subset of control sessions (four sessions for Y, nine sessions for G), 5 μl of saline solution was injected instead of muscimol. Contrasting the muscimol inactivation data to the saline control data produced the same results as contrasting the muscimol inactivation data to all control data (Figure S4C).

Behavioral Tasks

The monkeys sat in a dark room ~40 cm in front of an LCD monitor mounted behind a touch-sensitive screen and made center-out reach or saccade movements in their frontoparallel plane. Because of the backlight of the LCD monitor, the hand near the monitor was visible. Eye position was tracked with an infrared eye tracker (ISCAN, 120 Hz). For a subset of data, the continuous hand position was also recorded using an optical motion tracking system (Northern Digital).

In a single session, the monkeys typically completed one of three different sets of experiments. Set 1 included the memory-guided reach and saccade tasks (seven controls and six inactivations for monkey Y, six and six for monkey G; Figure 2A). In all sessions, the monkeys performed both tasks, except for four control and three inactivation sessions in which monkey Y performed only the saccade but not the reach task. In both tasks, a trial began as the monkeys fixed their eyes on the central eye-fixation target and touched the central hand-fixation target. After 0.5 s of the central hold period, a target stimulus was presented in the periphery for 0.3 s, and a 1-s-long memory period followed the target stimulus offset. The memory period ended as the central hand-fixation target was extinguished, cueing the monkeys to move ("go" signal). In the reach task, the target was a green circle. In the saccade task, the target was a red square. Target locations were six evenly spaced points around the circle with the radius 7.26 cm for monkey Y and 8.25 cm for monkey G. If the monkeys initiated the instructed movement within 2 s from the go signal and the movement ended within a tolerance from the target, they received a drop of juice in 0.3 s after the movement end. The endpoint tolerance for the reach task was 4 cm in radius for both monkeys, while the tolerance for the saccade task was ~7° for monkey Y and ~9° for monkey G. The same tolerances for reaction times and the end points were used in both control and inactivation sessions. The tolerances were set leniently to observe behavioral consequences of the inactivation while suppressing error-based adaptations and to keep the monkeys motivated by minimizing the number of failed trials.

Set 2 tested the foveal versus extrafoveal reach tasks (seven controls and six inactivations for monkey Y, 13 and 12 for monkey G; Figure 3A). The extrafoveal reach task was similar to the reach task in set 1 but no memory period was interposed. After the central hold period, concurrently with the target presentation, the central hand-fixation target was extinguished, cueing the monkeys to move ("go" signal). Target locations were slightly different from those in the memory-guided reach task. The six targets were points around two concentric circles. The two targets directly to the right and left from the hand-fixation target were on the outer circle, while the targets in the four diagonal directions were on the inner circle. The radii of the inner and outer circles were 7.8 cm and 11.25 cm for monkey Y and 8.8 cm and 12.75 cm for monkey G. In the foveal reach task, the monkeys' eyes were not constrained in any way so that the monkeys showed typical eye-hand coordination (Figure 3B).

Set 3 tested the directly versus symbolically cued reach tasks (three controls and three inactivations for Y, three and four for G; Figure S2A). The direct task was identical to the extrafoveal reach task in set 2. The target locations were six evenly spaced points around the circle with the radius 9.4 cm for both monkeys. The symbolic task differed from the direct task only in the following way: after the central hold period, an arrow was presented in the central visual field instead of illuminating the target location in the periphery. The monkeys had to reach in the direction of the arrow, while fixating the eyes on the fixation target. To compute the reach end point error in the symbolic task, we used the target location in the direct task in the direction of the arrow.

All tasks tested six peripheral targets, three for each visual field. Different tasks and target locations were randomly interleaved. On average, 26 ± 11.3 successful movements per target and task condition were completed in each session.

Behavioral Data Analysis

We measured reaction time, movement time, movement amplitude, and end point variance of each trial based on the movement take-off and landing times and movement start and end points. In the reach trial, take-off was when the hand was lifted off from the touch-sensitive screen, and landing was when the hand touched the screen back. The movement start and end points were the hand positions registered on the screen just before take-off and just after landing, respectively. The movement amplitude was the Euclidian distance between the movement start and end points. The endpoint variance was the average of variances of the endpoints in x and y dimensions. The reaction time was the time elapsed from the go signal until take-off. The movement time was the time between take-off and landing. In the saccade trials, we measured the same four measures but the take-off and landing events were determined differently from the reach. Take-off was the first time when eye velocity fell below 10 cm/s (~14°/s) when going backward in time from peak velocity and landing was the first time when eye velocity fell below 10 cm/s (~14°/s) continuously over 50 ms when going forward.

Statistical Tests

First, we assessed the overall inactivation effect on a given task condition as follows. All trials were combined together across all inactivation and control sessions, respectively. Then, an unpaired two-sample t test was applied to the two populations, control and inactivation, to determine the statistical significance of the difference in their means (Figure 3C). Second, we assessed the inactivation effect on each task condition per target location. All trials in the same target location were pooled together across all inactivation sessions and across all control sessions, respectively. Then, an unpaired two-sample t test was applied to the two populations to determine the statistical significance of the difference in their means (Figures 2C and 2D). The significance level for multiple comparisons over the six target locations was adjusted using Bonferroni correction. When we compared the inactivation effect between any two task conditions or the two hemifields, we computed the reduction of the movement amplitude of each inactivation trial from its baseline. The baseline was the mean movement amplitude of all control trials at the same target location in the same task condition as the inactivation trial. Then, we computed the percent reduction of the inactivation trial as (baseline-reach amplitude of the inactivation trial)/baseline × 100%. The population of each task condition or each hemifield was constructed by pooling the percent reduction over all inactivation trials in the given task condition or the given hemifield. The statistical significance of the difference in the mean percent reduction was estimated by applying an unpaired two-sample t test to the two populations (Figure 4A).

Population Vector Model

Prior to the inactivation experiments, we examined the functional properties of neurons in the posterior parietal cortex using the reach and saccade tasks (described in section Behavioral tasks; Figure 2A). The majority of neurons in PRR showed spatial tuning to the impending reach target and spatial tuning was stronger for the reach target than the saccade target (Figure 1A). Sites fulfilling these criteria were found over a large area, reaching up to 10 mm from the inactivation cannula (Figure S3C). The distance from the inactivation

center to each spiking unit was approximated using the distance between the entrance positions of the electrode and the injection cannula measured on the dura.

The tuning curve of each spiking unit was computed as the mean firing rate between −0.4 and 0.1 s from movement onset for each of the six target locations. The tuning curve was normalized so that the maximum is 1, and the minimum is 0. The preferred direction was determined as the direction of the vector sum of the tuning curve (Georgopoulos et al., 1986). The population vector for each target location was constructed by summing the activity of all units, each represented as a vector pointing in its preferred direction, with the amplitude proportional to its tuning curve value for the given target location. We assessed how well the underlying neuronal population activity matched the inactivation effect as a function of distance from the inactivation cannula by estimating the population vector using units only within the specified distances (Figure S3D).

SUPPLEMENTAL INFORMATION

Supplemental Information includes four figures and one table and can be found with this article online at http://dx.doi.org/10.1016/j.neuron.2012.10.030.

ACKNOWLEDGMENTS

This work was supported by NIH grant EY013337, EY005522, and DARPA award N66001-10-C-2009. E.J.H. was supported by NIH Career Development Award K99 NS062894. We thank Dr. Igor Kagan and Dr. James Bonaiuto for the acquisition and processing of MR images, Dr. Bardia Behabadi for scientific discussion, Tessa Yao for editorial assistance, Kelsie Pejsa and Nicole Sammons for animal care, and Viktor Shcherbatyuk for technical assistance.

Accepted: October 1, 2012
Published: December 5, 2012

REFERENCES

Andersen, R.A., and Buneo, C.A. (2002). Intentional maps in posterior parietal cortex. Annu. Rev. Neurosci. *25*, 189–220.

Andersen, R.A., Snyder, L.H., Bradley, D.C., and Xing, J. (1997). Multimodal representation of space in the posterior parietal cortex and its use in planning movements. Annu. Rev. Neurosci. *20*, 303–330.

Arikan, R., Blake, N.M., Erinjeri, J.P., Woolsey, T.A., Giraud, L., and Highstein, S.M. (2002). A method to measure the effective spread of focally injected muscimol into the central nervous system with electrophysiology and light microscopy. J. Neurosci. Methods *118*, 51–57.

Astafiev, S.V., Shulman, G.L., Stanley, C.M., Snyder, A.Z., Van Essen, D.C., and Corbetta, M. (2003). Functional organization of human intraparietal and frontal cortex for attending, looking, and pointing. J. Neurosci. *23*, 4689–4699.

Batista, A.P., Buneo, C.A., Snyder, L.H., and Andersen, R.A. (1999). Reach plans in eye-centered coordinates. Science *285*, 257–260.

Battaglia-Mayer, A., Ferraina, S., Mitsuda, T., Marconi, B., Genovesio, A., Onorati, P., Lacquaniti, F., and Caminiti, R. (2000). Early coding of reaching in the parietooccipital cortex. J. Neurophysiol. *83*, 2374–2391.

Bisley, J.W., and Goldberg, M.E. (2010). Attention, intention, and priority in the parietal lobe. Annu. Rev. Neurosci. *33*, 1–21.

Blangero, A., Ota, H., Rossetti, Y., Fujii, T., Ohtake, H., Tabuchi, M., Vighetto, A., Yamadori, A., Vindras, P., and Pisella, L. (2010). Systematic retinotopic reaching error vectors in unilateral optic ataxia. Cortex *46*, 77–93.

Buxbaum, L.J., and Coslett, H.B. (1997). Subtypes of optic ataxia: Reframing the disconnection account. Neurocase *3*, 159–166.

Buxbaum, L.J., and Coslett, H.B. (1998). Spatio-motor representations in reaching: Evidence for subtypes of optic ataxia. Cogn. Neuropsychol. *15*, 279–312.

Caminiti, R., Chafee, M.V., Battaglia-Mayer, A., Averbeck, B.B., Crowe, D.A., and Georgopoulos, A.P. (2010). Understanding the parietal lobe syndrome from a neurophysiological and evolutionary perspective. Eur. J. Neurosci. *31*, 2320–2340.

Cavina-Pratesi, C., Monaco, S., Fattori, P., Galletti, C., McAdam, T.D., Quinlan, D.J., Goodale, M.A., and Culham, J.C. (2010). Functional magnetic resonance imaging reveals the neural substrates of arm transport and grip formation in reach-to-grasp actions in humans. J. Neurosci. *30*, 10306–10323.

Cisek, P., and Kalaska, J.F. (2004). Neural correlates of mental rehearsal in dorsal premotor cortex. Nature *431*, 993–996.

Colby, C.L., Gattass, R., Olson, C.R., and Gross, C.G. (1988). Topographical organization of cortical afferents to extrastriate visual area PO in the macaque: a dual tracer study. J. Comp. Neurol. *269*, 392–413.

Connolly, J.D., Andersen, R.A., and Goodale, M.A. (2003). FMRI evidence for a 'parietal reach region' in the human brain. Exp. Brain Res. *153*, 140–145.

Corbetta, M., Kincade, J.M., Ollinger, J.M., McAvoy, M.P., and Shulman, G.L. (2000). Voluntary orienting is dissociated from target detection in human posterior parietal cortex. Nat. Neurosci. *3*, 292–297.

Culham, J.C., Cavina-Pratesi, C., and Singhal, A. (2006). The role of parietal cortex in visuomotor control: what have we learned from neuroimaging? Neuropsychologia *44*, 2668–2684.

D'Esposito, M. (2003). Neurological Foundations of Cognitive Neuroscience (Cambridge, MA: MIT Press).

Filimon, F., Nelson, J.D., Huang, R.S., and Sereno, M.I. (2009). Multiple parietal reach regions in humans: cortical representations for visual and proprioceptive feedback during on-line reaching. J. Neurosci. *29*, 2961–2971.

Gallese, V., Murata, A., Kaseda, M., Niki, N., and Sakata, H. (1994). Deficit of hand preshaping after muscimol injection in monkey parietal cortex. Neuroreport *5*, 1525–1529.

Galletti, C., Fattori, P., Kutz, D.F., and Battaglini, P.P. (1997). Arm movement-related neurons in the visual area V6A of the macaque superior parietal lobule. Eur. J. Neurosci. *9*, 410–413.

Garcin, R., Rondot, P., and de Recondo, J. (1967). [Optic ataxia localized in 2 left homonymous visual hemifields (clinical study with film presentation)]. Rev. Neurol. (Paris) *116*, 707–714.

Georgopoulos, A.P., Schwartz, A.B., and Kettner, R.E. (1986). Neuronal population coding of movement direction. Science *233*, 1416–1419.

Gnadt, J.W., Bracewell, R.M., and Andersen, R.A. (1991). Sensorimotor transformation during eye movements to remembered visual targets. Vision Res. *31*, 693–715.

Gold, J.I., and Shadlen, M.N. (2007). The neural basis of decision making. Annu. Rev. Neurosci. *30*, 535–574.

Goodale, M.A., and Milner, A.D. (1992). Separate visual pathways for perception and action. Trends Neurosci. *15*, 20–25.

Green, A.M., and Angelaki, D.E. (2010). Multisensory integration: resolving sensory ambiguities to build novel representations. Curr. Opin. Neurobiol. *20*, 353–360.

Grefkes, C., and Fink, G.R. (2005). The functional organization of the intraparietal sulcus in humans and monkeys. J. Anat. *207*, 3–17.

Heiss, J.D., Walbridge, S., Asthagiri, A.R., and Lonser, R.R. (2010). Image-guided convection-enhanced delivery of muscimol to the primate brain. J. Neurosurg. *112*, 790–795.

Hwang, E.J., and Andersen, R.A. (2012). Spiking and lfp activity in PRR during symbolically instructed reaches. J. Neurophysiol. *107*, 836–849.

Hyvärinen, J. (1982). The Parietal Cortex of Monkey and Man (Berlin: Springer-Verlag).

Jackson, S.R., Newport, R., Mort, D., and Husain, M. (2005). Where the eye looks, the hand follows; limb-dependent magnetic misreaching in optic ataxia. Curr. Biol. *15*, 42–46.

Kalaska, J.F., Caminiti, R., and Georgopoulos, A.P. (1983). Cortical mechanisms related to the direction of two-dimensional arm movements: relations

in parietal area 5 and comparison with motor cortex. Exp. Brain Res. *51*, 247–260.

Karnath, H.-O., and Perenin, M.-T. (2005). Cortical control of visually guided reaching: evidence from patients with optic ataxia. Cereb. Cortex *15*, 1561–1569.

Khan, A.Z., Pisella, L., Vighetto, A., Cotton, F., Luauté, J., Boisson, D., Salemme, R., Crawford, J.D., and Rossetti, Y. (2005). Optic ataxia errors depend on remapped, not viewed, target location. Nat. Neurosci. *8*, 418–420.

Khan, A.Z., Blangero, A., Rossetti, Y., Salemme, R., Luauté, J., Deubel, H., Schneider, W.X., Laverdure, N., Rode, G., Boisson, D., and Pisella, L. (2009). Parietal damage dissociates saccade planning from presaccadic perceptual facilitation. Cereb. Cortex *19*, 383–387.

Levy, I., Schluppeck, D., Heeger, D.J., and Glimcher, P.W. (2007). Specificity of human cortical areas for reaches and saccades. J. Neurosci. *27*, 4687–4696.

Lewis, J.W., and Van Essen, D.C. (2000). Mapping of architectonic subdivisions in the macaque monkey, with emphasis on parieto-occipital cortex. J. Comp. Neurol. *428*, 79–111.

Li, C.S., Mazzoni, P., and Andersen, R.A. (1999). Effect of reversible inactivation of macaque lateral intraparietal area on visual and memory saccades. J. Neurophysiol. *81*, 1827–1838.

Liu, Y., Yttri, E.A., and Snyder, L.H. (2010). Intention and attention: different functional roles for LIPd and LIPv. Nat. Neurosci. *13*, 495–500.

Mantini, D., Hasson, U., Betti, V., Perrucci, M.G., Romani, G.L., Corbetta, M., Orban, G.A., and Vanduffel, W. (2012). Interspecies activity correlations reveal functional correspondence between monkey and human brain areas. Nat. Methods *9*, 277–282.

Martin, J.H., and Ghez, C. (1999). Pharmacological inactivation in the analysis of the central control of movement. J. Neurosci. Methods *86*, 145–159.

Mesulam, M.M. (2000). Principles of Behavioral and Cognitive Neurology (Oxford: Oxford University Press).

Milner, A.D., Paulignan, Y., Dijkerman, H.C., Michel, F., and Jeannerod, M. (1999). A paradoxical improvement of misreaching in optic ataxia: new evidence for two separate neural systems for visual localization. Proc. Biol. Sci. *266*, 2225–2229.

Mulliken, G.H., Musallam, S., and Andersen, R.A. (2008). Forward estimation of movement state in posterior parietal cortex. Proc. Natl. Acad. Sci. USA *105*, 8170–8177.

Murata, A., Gallese, V., Kaseda, M., and Sakata, H. (1996). Parietal neurons related to memory-guided hand manipulation. J. Neurophysiol. *75*, 2180–2186.

Perenin, M.T., and Vighetto, A. (1988). Optic ataxia: a specific disruption in visuomotor mechanisms. I. Different aspects of the deficit in reaching for objects. Brain *111*, 643–674.

Pesaran, B., Nelson, M.J., and Andersen, R.A. (2006). Dorsal premotor neurons encode the relative position of the hand, eye, and goal during reach planning. Neuron *51*, 125–134.

Pisella, L., Gréa, H., Tilikete, C., Vighetto, A., Desmurget, M., Rode, G., Boisson, D., and Rossetti, Y. (2000). An 'automatic pilot' for the hand in human posterior parietal cortex: toward reinterpreting optic ataxia. Nat. Neurosci. *3*, 729–736.

Prablanc, C., Pélisson, D., and Goodale, M.A. (1986). Visual control of reaching movements without vision of the limb. I. Role of retinal feedback of target position in guiding the hand. Exp. Brain Res. *62*, 293–302.

Prado, J., Clavagnier, S., Otzenberger, H., Scheiber, C., Kennedy, H., and Perenin, M.T. (2005). Two cortical systems for reaching in central and peripheral vision. Neuron *48*, 849–858.

Ratcliff, G., and Davies-Jones, G.A.B. (1972). Defective visual localization in focal brain wounds. Brain *95*, 49–60.

Rizzolatti, G., and Sinigaglia, C. (2010). The functional role of the parieto-frontal mirror circuit: interpretations and misinterpretations. Nat. Rev. Neurosci. *11*, 264–274.

Rossetti, Y., Pisella, L., and Vighetto, A. (2003). Optic ataxia revisited: visually guided action versus immediate visuomotor control. Exp. Brain Res. *153*, 171–179.

Saleem, K.S., and Logothetis, N.K. (2012). A Combined MRI and Histology Atlas of the Rhesus Monkey Brain in Stereotaxic Coordinates (London: Academic Press).

Schindler, I., Rice, N.J., McIntosh, R.D., Rossetti, Y., Vighetto, A., and Milner, A.D. (2004). Automatic avoidance of obstacles is a dorsal stream function: evidence from optic ataxia. Nat. Neurosci. *7*, 779–784.

Snyder, L.H., Batista, A.P., and Andersen, R.A. (1997). Coding of intention in the posterior parietal cortex. Nature *386*, 167–170.

Trillenberg, P., Sprenger, A., Petersen, D., Kömpf, D., Heide, W., and Helmchen, C. (2007). Functional dissociation of saccade and hand reaching control with bilateral lesions of the medial wall of the intraparietal sulcus: implications for optic ataxia. Neuroimage *36*(*Suppl 2*), T69–T76.

Vesia, M., Prime, S.L., Yan, X., Sergio, L.E., and Crawford, J.D. (2010). Specificity of human parietal saccade and reach regions during transcranial magnetic stimulation. J. Neurosci. *30*, 13053–13065.